Mathematical Medicine and Biology (2010) **27**, 211–225
doi:10.1093/imammb/dqp019
Advance Access publication on October 27, 2009

A model for wetting and evaporation of a post-blink precorneal tear film

KATLYN N. WINTER† AND DANIEL M. ANDERSON‡
Department of Mathematical Sciences, George Mason University, Fairfax, VA 22030, USA

AND

RICHARD J. BRAUN§
Department of Mathematical Sciences, University of Delaware, Newark, DE 19716, USA

[Received on 18 March 2009; revised on 31 July 2009; accepted on 24 August 2009]

We examine a fluid dynamic model for the evolution of a precorneal tear film that includes evaporation of the aqueous layer and a wetting corneal surface. Our model extends previous work on the break-up time for a post-blink tear film to include a more realistic model for evaporation. The evaporation model includes the effects of conjoining pressure and predicts the existence of an equilibrium adsorbed fluid layer that serves as a model for a wetting corneal surface/mucin layer. The model allows the prediction of dewetting rates that are compared with experimental measurements. By choosing an expected thickness where evaporation and conjoining pressure balance, we obtain qualitative agreement for the opening rate with *in vivo* observations.

Keywords: tear film; evaporation; van der Waals; wetting.

1. Introduction

After each blink, a thin fluid film covers the surface of the eye. This thin film contributes to the optical function of the eye, protects the corneal surface and provides a lubricating layer that helps prevent irritation of the eyelid rubbing on the eye during a blink. Millions of people suffer from a collection of symptoms called dry eye in which the tear film does not properly execute its manifold functions (Smith *et al.*, 2007). For example, in Sjögren's syndrome, the immune system may attack the moisture producing glands in the body, such as the salivary glands in the mouth and the lacrimal glands near the eye. This is just one cause for insufficient tear production, which may in turn lead to the dryness, irritation, gritty sensation or other symptoms of dry eye. The tear film may also evaporate too rapidly due to malfunction of the meibomian glands in the eyelids, which produce a protective oily layer of lipids that help preserve the tear film (Mishima & Maurice, 1961; Mathers, 2004). The most up-to-date report on dry eye may be found in the Dry Eye Workshop report (Lemp *et al.*, 2007). Mathematical models offer the possibility of improved understanding of normal, healthy tear dynamics as well as varying the amount and properties of the tear film to better understand unhealthy situations.

A classic characterization of the human tear film is one consisting of three distinct layers: the lipid layer, the aqueous layer and the mucus layer. More recent views on the detailed make-up of the tear film

†Email: katlynwinter@gmail.com
‡Corresponding author. Email: danders1@gmu.edu
§Email: braun@math.udel.edu

reveal a considerably more complicated picture. Even the seemingly simple measurement of the overall thickness of the tear film is a challenging problem. The reported overall thickness of the tear film ranges from a few microns to tens of microns (e.g. Bron *et al.*, 2004), with more recent measurements based on interferometry suggesting values in the lower end of this range (e.g. 1.5–4.7μm; King-Smith *et al.*, 2000). Measurements via optical coherence tomography confirm this result (Wang *et al.*, 2003). For a review, see King-Smith *et al.* (2004).

The lipid layer, composed mainly of meibomian lipid secreted from the meibomian glands, has a thickness typically 100 nm or less and plays numerous roles in the overall function of the tear film (for a review, see Bron *et al.*, 2004). From a fluid dynamic point of view, the lipid film's higher viscosity and lower surface tension help stabilize the tear film. The presence of the lipid layer also reduces evaporation of the aqueous fluid in the tear film. For example, patients with meibomian gland disfunction show elevated rates of evaporation up to several times larger than that for a normal eye (Bron *et al.*, 2004).

The existence of distinct aqueous and mucus layers has more recently come into question. While quoted values for the thicknesses of the aqueous layer (e.g. 4–10 μm; Mishima, 1965; Sharma, 1998) and mucus layer (e.g. 1 μm; Wong *et al.*, 1996; Sharma *et al.*, 1999, and references therein) have been reported, more recent reviews suggest that the three-layer theory should be replaced by one in which the mucins are mixed throughout a mucoaqueous layer (Gipson, 2004; Bron *et al.*, 2004; Cher, 2007). The view of Gipson (2004) reveals an intricate picture of the mucoaqueous tear film and the corneal surface. In this view of the mucoaqueous layer, both gel-forming and transmembrane mucins are present. The secreted mucins mix with the aqueous layer and are thought to serve a variety of purposes such as debris removal and tear film stabilization. A detailed view of the corneal surface reveals a complex picture. Transmembrane mucins 200–500 nm long extend as rod-like structures from the corneal surface, which itself has microplicae a few hundred nanometres tall. The hydrophilic nature of the mucins and the complicated cellular structures of the cornea point to a surface that is wetting (Bron *et al.*, 2004; Gipson, 2004), which is one of the operating assumptions for our model corneal surface.

Our objective in the present work was to examine a model for a human tear film that treats the corneal surface as a wettable surface on which rupture never occurs but instead on which a stable adsorbed fluid layer remains after thinning due to relaxation and evaporation. The transmembrane and gel-forming mucins near the corneal surface are assumed to remain hydrated thus preventing a true dryout on time scales that are not too long. When the tear film thins to such a degree, it is expected that the osmolarity (concentration of salts) of the film increases and that hyperosmolarity is an important factor in dry eye and related symptoms (Lemp *et al.*, 2007; Klyce & Russell, 1979; Levin & Verkman, 2004). A recent compartment-based model has studied this aspect of the anterior eye (Bron *et al.*, 2008); however, we neglect any description of the osmolarity in this work.

Our mathematical model combines the tear film model of Braun & Fitt [2003; hereafter referred to as the constant evaporation rate (CER) model] with the incorporation of a new evaporation model based on the work of Ajaev (2005b) and Ajaev & Homsy (2001). This evaporation model incorporates pressure effects (in addition to thermal effects) and a conjoining pressure derived from the work of Wu & Wong (2004). The inclusion of these effects into the CER model allows for the existence of a wetting layer with a physiologically reasonable thickness on the corneal surface. Furthermore, the tear film dynamics in the present model can now be examined beyond the predicted rupture times of the CER model and, consequently, may be used as a basis to explore opening rates of holes or 'dry' spots on the corneal surface. Finally, we note that while the tear film is reported to have non-Newtonian properties (Tiffany, 1991; Zhang *et al.*, 2003a) , we shall neglect these effects here and treat the fluid in our tear film model as Newtonian.

Our paper is organized as follows. In Section 2, we formulate the tear film model with an improved evaporation treatment. The governing equations and their reduction to a single evolution equation using lubrication theory are given in this section. Results focusing on the new evaporation terms and the implications for tear films are given in Section 3. Conclusions are given in Section 4.

2. Formulation

We model the tear film as an incompressible Newtonian fluid with constant density ρ, dynamic viscosity μ, specific heat c_p and thermal conductivity k. The tear film geometry is defined by the domain $0 < y < h(x,t)$ with eyelids at the ends of the domain $-L < x < L$. We address only the dynamics of a post-blink tear film so that the eyelid positions are fixed in time. The governing equations are given by

$$\nabla \cdot \boldsymbol{u} = 0, \tag{1}$$

$$\rho\left(\frac{\partial \boldsymbol{u}}{\partial t} + \boldsymbol{u}\cdot\nabla\boldsymbol{u}\right) = -\nabla p + \mu\nabla^2\boldsymbol{u} + \rho g\hat{\mathbf{i}}, \tag{2}$$

$$\rho c_p\left(\frac{\partial T}{\partial t} + \boldsymbol{u}\cdot\nabla T\right) = k\nabla^2 T, \tag{3}$$

where $\boldsymbol{u} = (u, v)$ is the 2D velocity vector, p is the fluid pressure in the film, T is the temperature and g is the gravitational acceleration.

The above governing equations are subject to boundary conditions at the corneal surface at $y = 0$

$$u = v = 0, \quad T = T_{\text{eye}}, \tag{4}$$

where T_{eye} is assumed to be a prescribed constant temperature. We note that the central ocular surface temperature is known to decrease by about 1–1.5°C after a blink; for a recent review of measurement techniques and results, see Purslow & Wolffsohn (2005). We wish to keep the model as simple as possible in order to explore the effects of evaporation competing with conjoining pressure; we choose to neglect this surface cooling in this work. At the tear film–vapour interface $y = h(x,t)$, we impose boundary conditions associated with balance of mass, balance of normal stress, tangential fluid velocity, heat flux balance and a constitutive law for the evaporative mass flux J. The mass balance is

$$J \equiv \rho(\boldsymbol{u} - \boldsymbol{u}_{\text{I}})\cdot\hat{\mathbf{n}} = \frac{\rho(v - uh_x - h_t)}{(1+h_x^2)^{1/2}}, \tag{5}$$

where $\boldsymbol{u}_{\text{I}} = h_t\hat{\mathbf{k}}$ is the velocity of the interface. The normal stress balance is

$$-p_v - \hat{\mathbf{n}}\cdot\mathbf{T}\cdot\hat{\mathbf{n}} = \gamma\,\nabla\cdot\hat{\mathbf{n}} - \Pi^*, \quad \text{with } \mathbf{T} = -p\mathbf{I} + \mu(\nabla\boldsymbol{u} + \nabla\boldsymbol{u}^T), \tag{6}$$

where $\mathbf{T}$ is the Newtonian stress tensor for the fluid and γ is the (assumed constant) surface tension. Π^* is the conjoining pressure in the film given by

$$\Pi^* = \frac{1}{h^3}[A^* + B^*(2hh_x^2h_{xx} - h_x^4)], \tag{7}$$

where A^* and B^* are constants (see Wu & Wong, 2004). When $B^* = 0$, this form reduces to the standard van der Waals force with Hamaker constant A^*. The case $B^* = 0$ represents the perfectly wetting case

and $B^* \neq 0$ represents the partially wetting case (Ajaev, 2005b). A number of other authors have studied problems specifically for tear film rupture driven by van der Waals forces, or disjoining pressure, as defined by reaching zero thickness for a film (e.g. Sharma & Ruckenstein, 1985; Zhang *et al.*, 2003a,b, 2004; Gorla & Gorla, 2004). Though Zhang *et al.* (2003a,b, 2004) studied multilayer films together with van der Waals forces, and their work helps inform our choices, we note that the underlying assumptions and layers dealt with in the models we propose are different than in those works. The choice of van der Waals term that we use will cause a conjoining pressure, indicating that the healthy cornea is wettable (e.g. Bron *et al.*, 2004) rather than the non-wetting case that has been used previously based on what had been prevailing wisdom. We treat only the uniformly healthy cornea here, but we note that the incorporation of varying wettability on the substrate in order to represent unhealthy parts of the cornea may be a profitable direction (e.g. Thiele *et al.*, 2003; Sharma, 2003).

The lipid layer is a highly viscous layer (Tiffany, 1987) with an insoluble surfactant at the lipid–aqueous interface (McCulley & Shine, 1997). Previous works have shown that a limiting case of the strong insoluble surfactant for a film with moving ends is the uniform stretching limit (Jones *et al.*, 2005; Braun & King-Smith, 2007); for the case with stationary ends, this limit reduces to the tangentially immobility condition

$$\boldsymbol{u} \cdot \hat{\mathbf{t}} = 0. \tag{8}$$

This limit was first employed in Wong *et al.* (1996) and has been used in many eye-related studies since; it is also possible to obtain this limit for large surface viscosity as in Naire *et al.* (2000). Due to space considerations, we simply assume this end result rather than repeating these or similar derivations here. The review by Tiffany (1987) suggests that *in vitro* measurements indicate a roughly linear dependence of evaporation rate on the lipid thickness over the range of 50–200 nm. In the present context, we model an insoluble surfactant to be strong and in effect the lipid layer immediately becomes uniform spatially. We therefore neglect any variation of the evaporation on lipid film thickness when the eyelids do not move.

The heat flux balance is given by

$$-k\hat{\mathbf{n}} \cdot \nabla T = L_m J, \tag{9}$$

where L_m is the latent heat of vapourization per unit mass. Note the above equations are the so-called one-sided model of Burelbach *et al.* (1988) where the effects such as vapour viscosity and vapour thermal conductivity are neglected. In their full model effects related to the liquid–vapour density difference, such as vapour recoil, are retained. However, we follow the CER model and neglect this effect in the present tear film model. The unit normal and tangential vectors to the interface $\hat{\mathbf{n}}$ and $\hat{\mathbf{t}}$ are

$$\hat{\mathbf{n}} = \frac{(-h_x, 1)}{(1 + h_x^2)^{1/2}}, \quad \hat{\mathbf{t}} = \frac{(1, h_x)}{(1 + h_x^2)^{1/2}}. \tag{10}$$

The above equations are to this point equivalent to those of the CER model if the conjoining pressure Π^* is zero.

The CER model took the evaporative mass flux proportional to the difference between the interface temperature T_i and the equilibrium saturation temperature T_s (see Burelbach *et al.*, 1988). In the present work, we follow Ajaev & Homsy (2001) and Ajaev (2005b) and take the mass flux to be of the form

$$KJ = \alpha(p - p_v) + T_\mathrm{i} - T_\mathrm{s}, \tag{11}$$

where K and α are constants. This form of the mass flux allows for deviations in temperature and pressure to drive evaporation. Including a conjoining pressure with this evaporation model leads to the possibility of an equilibrium adsorbed liquid film on the corneal surface in which the mass flux is zero and evaporation is effectively shut off. Our one-sided tear film model with thermal and pressure-driven mass flux treats evaporation differently than the diffusion-limited model explored by Creech *et al.* (1998). Their 1D diffusion-limited vapour-phase evaporation model predicted tear film thinning rates comparable with the experimentally measured thinning rates of 0.5 μm min^{-1} of Rolando & Refojo (1983). However, more recent data by King-Smith *et al.* (2008, 2009) suggest evaporation rates 8–10 times larger than that shown in the data of Rolando and Refojo. This new evidence suggests a considerably faster evaporation rate not captured by a diffusion-limited process through the vapour phase but to which the present evaporation parameters can be effectively fit. We emphasize that the new features of the tear film model incorporate a wettable corneal surface and allow our numerical calculations to be extended beyond the predicted rupture time of the CER model.

We follow the CER model and introduce dimensionless variables of the form

$$x = l\bar{x}, \quad y = d\bar{y}, \quad t = \frac{l}{U_0}\bar{t}, \tag{12}$$

$$h = d\bar{h}, \quad u = U_0\bar{u}, \quad v = \epsilon U_0\bar{v}, \quad p = \frac{\mu U_0}{l\epsilon^2}\bar{p}, \quad \theta = \frac{T - T_\text{s}}{T_\text{eye} - T_\text{s}}, \quad J = \frac{k}{dL_m}(T_\text{eye} - T_\text{s})\bar{J}, \tag{13}$$

where $\epsilon = d/l$ represents a ratio of typical vertical to horizontal length scales which we shall assume to be small. Suitable values for length scale l and velocity scale U_0 depend on the value of d as shown by Braun & Fitt (2003); they chose $l = [d\gamma/(\rho g)]^{1/3}$ and $U_0 = \rho g d^2/\mu$. In their work, $d = 10\mu\text{m}$ which gave $l = 360\mu\text{m}$ and $U_0 = 755\mu\text{m s}^{-1}$. More recent evidence suggests smaller values of d. In our work, we also examine $d = 5\mu\text{m}$ ($l = 284\mu\text{m}$ and $U_0 = 189\mu\text{m s}^{-1}$) as well as $d = 3\mu\text{m}$ ($l = 240\mu\text{m}$ and $U_0 = 84\mu\text{m s}^{-1}$). These correspond to time scales $l/U_0 = 0.48$ s ($d = 10\mu\text{m}$), 1.5 s ($d = 5\mu\text{m}$) and 2.9 s ($d = 3\mu\text{m}$).

The above non-dimensionalization leads to a system in which we investigate the thin film limit $\epsilon \ll 1$. A depth-averaged evolution equation for the tear film thickness can be obtained through the application of lubrication theory (e.g. Wong *et al.*, 1996; Sharma *et al.*, 1998; Braun & Fitt, 2003; Ajaev, 2005b). We follow the assumptions of Braun and Fitt and take $l = d^{1/3}D^{2/3}$, where $D = \sqrt{\gamma/\rho g}$ and $U_0 = \rho g d^2/\mu$ so that $Ca = \mu U_0/(\gamma\epsilon^3) = 1$. This leads to the evolution equation for the tear film thickness

$$\frac{\partial h}{\partial t} + \frac{E}{\bar{K} + h}\left[1 - \delta\left(\frac{\partial^2 h}{\partial x^2} + \Pi\right)\right] = -\frac{\partial}{\partial x}\left\{\frac{h^3}{12}\left(\frac{\partial^3 h}{\partial x^3} + \frac{\partial \Pi}{\partial x} + G\right)\right\}, \tag{14}$$

where the dimensionless conjoining pressure term is given by

$$\Pi = \frac{1}{h^3}[A + B(2hh_x^2 h_{xx} - h_x^4)], \tag{15}$$

and the associated dimensionless parameters are given by

$$A = \frac{A^*}{\mu U_0 d l}, \quad B = \epsilon^4\frac{B^*}{\mu U_0 d l}, \quad G = \frac{\rho g d^2}{\mu U_0}, \tag{16}$$

$$E = \frac{k(T_\text{eye} - T_\text{s})}{\epsilon d L_m}, \quad \bar{K} = \frac{kK}{dL_m}, \quad \delta = \frac{\alpha\mu U_0}{\epsilon^2 l(T_\text{eye} - T_\text{s})}. \tag{17}$$

We point out that the Ajaev model for evaporation leads to an important term not present in the CER model that allows for the existence of an equilibrium adsorbed liquid film on the corneal surface consistent with a characterization of the corneal surface as a wetting surface. In this context, the dimensionless mass flux takes the form

$$J(x,h,t) = \frac{1}{\bar{K}+h}\left[1-\delta\left(\frac{\partial^2 h}{\partial x^2}+\Pi\right)\right], \tag{18}$$

which is represented in the evaporative term in (14).

When $\delta = 0$, $A = 0$ and $B = 0$, (14) reduces to the CER model [see Braun & Fitt, 2003, equation (42)]. For boundary and initial conditions, we focus on the new terms in this tear film model and consider exclusively conditions of fixed menisci height and fixed menisci curvature at the eyelids, respectively,

$$h(\pm L,t) = h^0 \quad \text{and} \quad h_{xx}(\pm L,t) = h^0_{xx}. \tag{19}$$

The initial conditions approximate the geometry of a post-blink tear film with a uniform central region of thickness $h_{\min}$ between two parabolic menisci at the upper and lower lids

$$h(x,t=0) = \begin{cases} h_{\min} & \text{if } |x| < L - \Delta x_m, \\ h_{\min} + \Delta h_m\,(|x| - (L-\Delta x_m))^2 & \text{if } |x| \geqslant L - \Delta x_m. \end{cases} \tag{20}$$

3. Results

We have implemented a method of lines approach to solve the tear film (14) where conservative central differencing in space is used to discretize the spatial terms at points $x_j = -L + 2L(j-1)/N$ for $j = 1,\ldots,N+1$. In all cases, boundary conditions $h(x=\pm L) = h^0$ and $\partial^2 h/\partial x^2(x=\pm L) = h^0_{xx}$ were used. The resulting system of ordinary differential equations in time were solved using Matlab's `ode23s` solver. In all calculations shown, we have used $N = 2000$ which we found to provide sufficient numerical accuracy.

Unless otherwise noted, the parameter values used in the present calculations are $L = 14$, $h^0 = 9$, $h^0_{xx} = 4$, $h_{\min} = 1$, $\Delta h_m = 2$, $\Delta x_m = 2$, $G = 0$, $E = 14.1$ and $K = 4930$, which are consistent with choices used in the CER model. Our focus in this paper will be to examine the effects of the parameters δ, A and B associated with the present evaporation and wetting model.

Figure 1 shows tear film profiles that include evaporative effects associated with interface curvature but without van der Waals effects. As we quantify further in Fig. 3 the inclusion of the new curvature term in the evaporative flux leads to negligible departures from the CER model with otherwise the same parameter values (cf. Braun & Fitt, 2003, Fig. 7). The dimensionless break-up time (BUT) for the film shown in Fig. 1 is slightly larger than 82 (approximately 40 s based on the time scale for $d = 10\mu$m).

Including van der Waals attractions together with the new curvature term is significant, however. Figure 2 shows the tear film profiles that include both effects. Note that in contrast to Fig. 1, evaporation is slowed considerably as the tear film thins, and the film reaches an equilibrium thickness equal to $h_{\text{eq}} = (\delta A)^{1/3}$. When the film reaches this equilibrium thickness, evaporation is locally zero; similar behaviour was seen by Ajaev (2005a,b). The tear film continues to evaporate in the thicker regions. A final equilibrium configuration is reached in which the thickness away from the meniscus regions reaches h_{eq}.

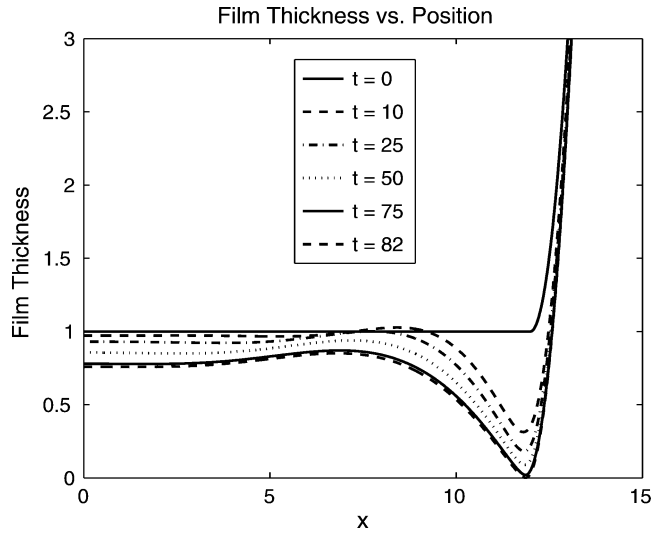

FIG. 1. This figure shows the shape of the thin tear film for designated time steps as indicated. Here, $\delta = 10^{-3}$, $A = 0$ and $B = 0$.

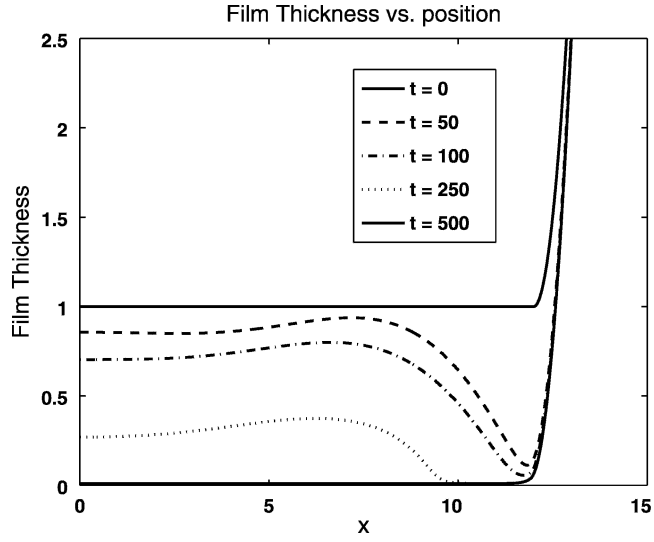

FIG. 2. This figure shows the shape of the thin tear film for designated time steps as indicated. Here, $\delta = A = 10^{-3}$ and $B = 0$.

In order to quantify the various effects in the present evaporation model and to compare with existing models, in Fig. 3, we track the minimum values of the film thickness at each time step. For the basic reference case (thin solid curve), all parameter values are set to 0 ($E = \delta = A = B = G = 0$) meaning the only acting forces are due to surface tension and viscosity. Here, the tear film thins on a relatively long scale. Next, we compare this case to the case in which the only additional non-zero terms are the van der Waals forces, $A = 10^{-3}$ (uppermost dash dotted curve) with no evaporation. By comparing these two results, we see that including van der Waals forces slows the thinning of the film. When the

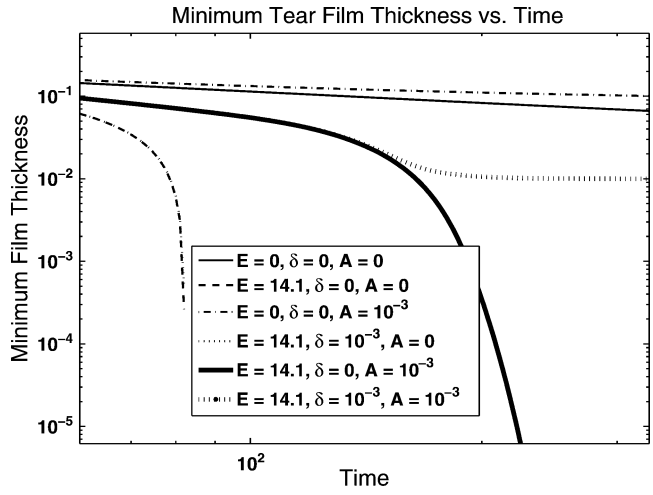

FIG. 3. This graph is a log–log plot of the minimum film thickness versus time for several representative cases.

CER model is examined (innermost dashed curve which is coincident with a dotted curve), there is a dramatic change in the thinning process and break-up is predicted to be around $t = 82$. This case does not include van der Waals forces or pressure effects in evaporation. Using $\delta = 10^{-3}$ has a negligible change from the CER prediction, also predicting a BUT of about 82. In these cases, the only parameter difference is that curvature effects are included in the evaporation term. While there is little difference between these two cases, the inclusion of the δ term results in a film that thins slightly more slowly. Another case is shown by the thick solid line that includes van der Waals forces, with $A = 10^{-3}$, added to the constant evaporation case (with $\delta = 0$). The BUT for this case is increased to about $t = 300$. This is the same general trend noted between the two non-evaporative curves (thin solid and thin dash dotted curves); i.e. when van der Waals forces are included, thinning is slowed and BUTs are increased. Last, we include a case with parameter values, $E = 14.1$, $A = \delta = 10^{-3}$ and $B = 0$ (short dashed line). Notice as $t \to \infty$, the curve levels off to an equilibrium thickness. This is due to the van der Waals forces term in the evaporative mass flux that effectively shuts off evaporation when $h = h_{\text{eq}}$.

In Fig. 4 we examine in more detail the dependence of the evaporative dynamics on the parameters δ and A. Here, we plot the minimum film thickness as a function of time over a representative set of parameter values. We note that the predicted equilibrium film thickness, $(\delta A)^{1/3}$, agrees with the numerically obtained values shown as $t \to \infty$. Notice as the equilibrium film thickness gets smaller, the time in which this value is reached decreases. This general trend was also noticed when A and δ were varied independently. We note that the equilibrium film thickness does not depend on the value of B.

To better understand the effects in the evaporation term, we define and examine an evaporative flux multiplier function

$$Q_{\text{E}}(x,t) \equiv 1 - \delta\left(\frac{\partial^2 h}{\partial x^2} + \Pi\right). \tag{21}$$

Figure 5 reveals that when $\delta = 10^{-3}$ and $A = B = 0$, there is little variation; $Q_{\text{E}} \approx 1$ for all times. This shows why our previous observations indicated very little difference between the CER model and the present one with $\delta \neq 0$ but $A = B = 0$.

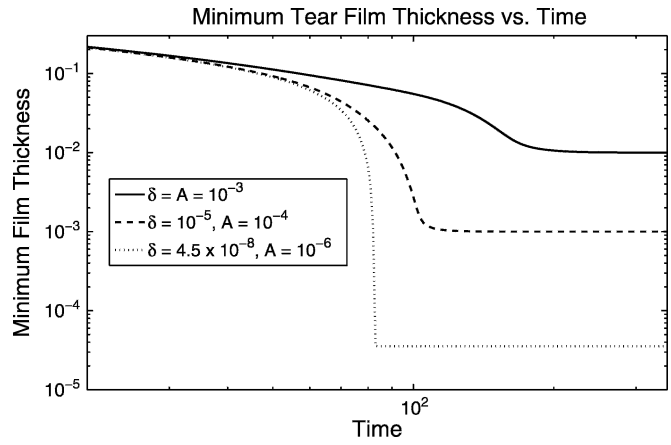

FIG. 4. This figure shows the minimum film thickness as a function of time for different values of parameters δ and A as indicated. Note that the equilibrium film thickness computed is consistent with the prediction $h_{\text{eq}} = (\delta A)^{1/3}$.

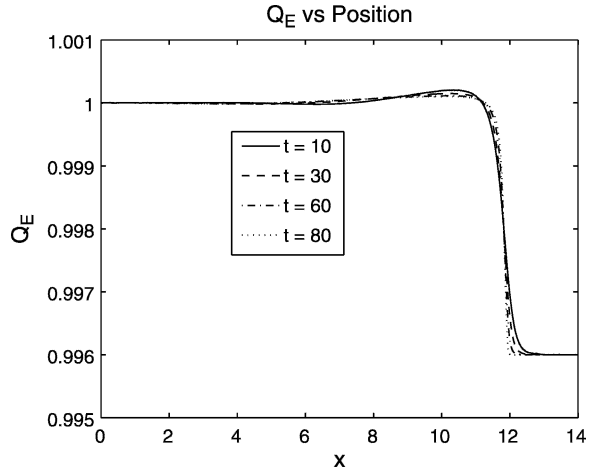

FIG. 5. Evaporative flux function $Q_{\text{E}}(x, t)$ profiles for different values of time. Here, $\delta = 10^{-3}$, $A = 0$ and $B = 0$.

Figure 6 shows $Q_{\text{E}}(x, t)$ for a range of time values for which the equilibrium film thickness is reached in various locations along the corneal surface. Here, both δ and A are non-zero. This plot reveals that Q_{E} becomes extremely small or even 0 for some spatial values, meaning that evaporation is shut off in those regions where the film reaches its equilibrium thickness. The signature of this shutting off of the evaporation is the levelling off of the minimum film thickness curves in Figs 3 and 4. In the plot of the corresponding film profiles in Fig. 7, we see the various regions of equilibrium film thickness.

Figure 7 reveals the late stages of the wetting dynamics of the film. The tear film evaporates locally until the equilibrium height $h_{\text{eq}} = (\delta A)^{1/3}$ is reached. At this point, the evaporation shuts off locally and the corneal surface remains wetted. At $t = 325$, there is an equilibrium adsorbed fluid layer between the meniscus at the eyelid (on the right) and the central region (on the left) for x between approximately 8 and 12. At this point, we identify two contact line positions $x = w_1(t)$ on the right (at the bottom of the

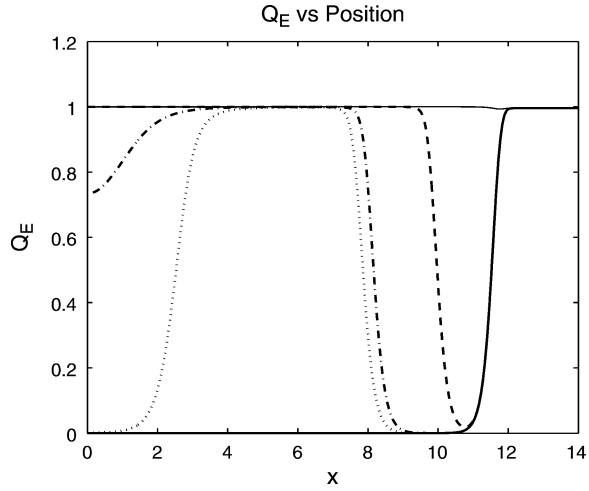

FIG. 6. Evaporative flux function $Q_E(x, t)$ profiles for different values of time. Here, $\delta = A = 10^{-3}$ and $B = 0$.

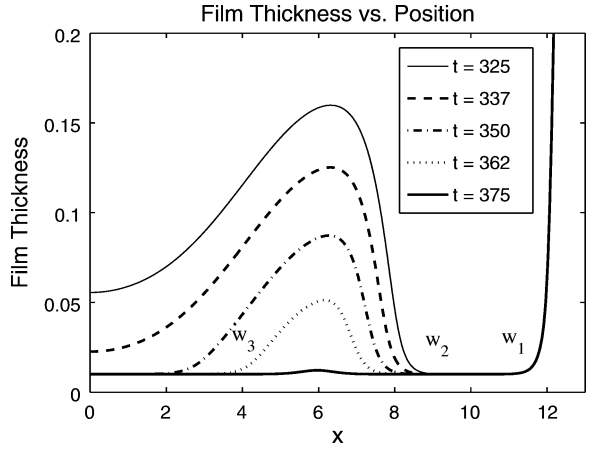

FIG. 7. Here, we plot the tear film profiles with $\delta = A = 10^{-3}$ and $B = 0$ over the time interval $t = 325$–375 showing evaporation of the bulk tear film. We can identify three contact lines in this figure: w_1 is effectively stationary near $x = 12$, w_2 moves to the left and at the early times shown in this figure is located near $x = 8$ and w_3 starts at the center ($x = 0$) and moves to the right eventually merging with w_2. Details of the dynamics of contact lines w_2 and w_3 are shown in the next figure.

meniscus) and $x = w_2(t)$ at the edge of the receding film near $x = 8$. As the film evolves further in time, a new adsorbed layer forms (shortly after $t = 337$) in the (symmetric) centre of the tear film (at $x = 0$) and gives rise to a third contact line $x = w_3(t)$ moving out away from the midpoint of the symmetric film. This smaller island of fluid eventually disappears (just after $t = 375$) leaving an adsorbed fluid layer on the surface and meniscus regions near the eyelids.

We next examine evolution of the dry regions of the corneal surface as was done for a similar model by Ajaev (2005a). Figure 8 shows the contact line positions as a function of time for two moving contact lines in Fig. 7. Additionally, we have included overall linear fits of the contact line dynamics to estimate the average velocities of these two contact lines w_2 and w_3. The contact line near the meniscus

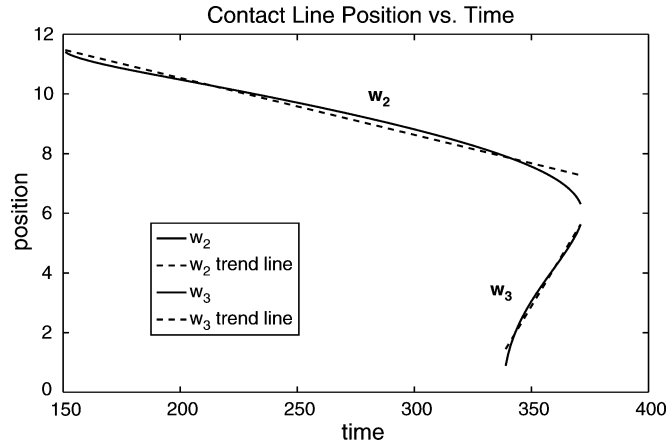

FIG. 8. Here, we plot the contact line positions $w_2(t)$ and $w_3(t)$ for the case $\delta = A = 10^{-3}$ and $B = 0$.

$x = w_1(t)$ is essentially stationary. In order to identify these curves and the corresponding linear fits to estimate contact line speed, we have defined the contact line positions w_2 and w_3 as the location at which the bulk fluid has a depth twice the thickness of the adsorbed fluid layer; i.e. where the film thickness is $2(\delta A)^{1/3}$. Other definitions may alter quantitatively the prediction of the contact line position, although the general contact line speed estimates based on this definition are robust. If we take 350 to be a dimensionless time for complete evaporation and length and time scales to be 10μm and 0.48 s, an estimate for the thinning rate of the tear film is approximately 3.6μm min^{-1}. This is slightly smaller than, but still close to, the average thinning rate of 3.79 μm min^{-1} measured by King-Smith *et al.* (2008).

The values of the average speeds indicated in Fig. 8 as well as equilibrium film thicknesses $h_{\text{eq}} = (\delta A)^{1/3}$ for various parameter values are listed in Table 1. We note that one interpretation of this equilibrium film thickness is the length scale of the structure of the corneal surface whose thickness we estimate to be approximately 0.3μm (see Gipson, 2004). We have examined a range of parameters that correspond to equilibrium film thicknesses up to this estimate. Below we compare these predictions to *in vivo* data.

We have been able to examine *in vivo* data of the break-up of a human precorneal tear film in video images provided to us by King-Smith. These video images show an illuminated 7-mm-diameter region of one patient's tear film for a duration of approximately 30 s following a blink. Superimposed on the images is a spatial grid with approximately $0.24 \times 0.24\ \text{mm}^2$. From these video images, we could obtain both qualitative and quantitative information on the precorneal tear film dynamics and break-up.

For this particular patient, several regions in the tear film could be clearly identified as locations where break-up was occurring. Generally, after an initial regime in which a roughly circular hole in the tear film forms, break-up areas were irregularly shaped rather than radially symmetric. In some cases, the break-up patches appeared more square or rectangular in shape. The merging of multiple nearby rupture patches was also observed. In certain instances, one can observe what appear to be capillary ridges near the break-up region which grow and shrink at different times. Some of the irregular structures observed in the tear film and rupture areas are likely related to irregularities of the underlying substrate (corneal) topography. Finally, the opening rates were observed to vary during break-up and in some cases, the opening process appears to reverse.

TABLE 1 *Equilibrium adsorbed film thickness and contact line speed estimates for two moving contact lines such as those observable in Fig. 7. The dimensional form of the equilibrium thickness is* $h_{eq} = (\delta A)^{1/3}d$. *The velocity scale* U_0 *has been computed using the formula* $U_0 = \rho g d^2/\mu$ *from Braun & Fitt (2003) with* $\rho = 10^3$ *kg* m^{-3}, $g = 9.81$ *m* s^{-2} *and* $\mu = 1.3 \times 10^{-3}$ *Pa s; they used* $d = 10\mu m$ *but we also include results for* $d = 5$ *and* $3\mu m$ *here. The parameter values* δ *and* A *were chosen to obtain dimensional equilibrium film thickness values around but also on either side of* $0.1\mu m$. *In the last case shown, the hole opening up from the centre of the tear film corresponding to contact line* $w_3(t)$ *is absent*

δ	A	B	d (μm)	h_{eq} (μm)	U_0 (μm s^{-1})	$w_2'(t)$ (μm s^{-1})	$w_3'(t)$ (μm s^{-1})
10^{-3}	10^{-3}	0	10	0.1	755	−14.4	98.6
10^{-5}	10^{-4}	0	10	0.01	755	−10.3	97.8
10^{-3}	10^{-3}	10^{-4}	10	0.1	755	−14.4	98.6
10^{-2}	10^{-2}	0	5	0.23	189	−7.4	54.6
10^{-2}	10^{-3}	0	5	0.11	189	−3.4	24.3
10^{-3}	10^{-2}	0	5	0.11	189	−10.4	77.4
10^{-1}	10^{-2}	0	3	0.3	68	−1.4	14.0
10^{-2}	10^{-1}	0	3	0.3	68	−1.1	N/A

N/A: not applicable.

TABLE 2 *Estimates for diameter, time and opening rates of two break-up regions in a human precorneal tear film (numerical values based on analysis of video images provided by P. E. King-Smith)*

Location	Diameter (mm)	Absolute time (s)	Opening speed (mm s^{-1})
Lower left	0.24	7	N/A
	0.48	11	0.03
	0.60	19	0.008
	0.72	25	0.01
Middle left	0.24	23	N/A
	0.36	25	0.03
	0.48	26/27	0.03

N/A: not applicable.

The observed film and dryspot dynamics are clearly quite complicated and the quantitative identification of temporal and spatial features is difficult. With these complexities in mind, we have examined in more detail two particular tear film rupture, or break-up, areas in the data in an attempt to estimate effective diameters, times and opening speeds of these ruptured areas that can be compared with the predictions of our model. These measured values are summarized in Table 2.

The results of Table 2 indicate that, after formation and rapid opening of the dryspot, there is a time span on the order of seconds where an opening rate of approximately 0.03 mm s^{-1} (30μm s^{-1}) is observed. In the first example, the later time data suggest a somewhat slower opening rate. Again, we emphasize that since the dryspots were irregularly shaped, the values given for diameter are only rough estimates. Also, the speed in a given direction is not monotonic and may even reverse a little. Our

numerical values are based on estimates of an average area; however, the observation that the opening rates start out large and then decrease seems to be a robust feature observed qualitatively and estimated quantitatively.

The estimated values for opening rates are generally in the range of the $\mathrm{d}w_2/\mathrm{d}t$ and $\mathrm{d}w_3/\mathrm{d}t$ values indicated in Table 1. The dryspots observed *in vivo* were away from the black lines (the black line regions were not contained within the illuminated region of the tear film in the video images) and so in some sense, the opening rates should be compared with those for $\mathrm{d}w_3/\mathrm{d}t$. In the cases where a smaller d is used, the numbers for $\mathrm{d}w_3/\mathrm{d}t$ are quite close considering the approximate nature of the estimates. Of course, our theoretical predictions for the opening rates (see Fig. 8) are 1D and show no indication of slowing down. While the comparison is encouraging, there is still room for improvement.

4. Conclusions

Some prior mathematical modelling studies have incorporated the best available understanding from the eye community at the time, but if they did include van der Waals forces, then those forces caused dewetting from a corneal surface that was assumed to be non-wetting. In this work, we made different choices that included van der Waals forces that reflect a cornea that is wettable by tear fluid, in accord with modern understanding of the corneal surface (Bron *et al.*, 2004; Gipson, 2004). Evaporation is also argued to be important in recent work (King-Smith *et al.*, 2008).

The competition of van der Waals forces causing a conjoining pressure with evaporation from the tear film surface can balance each other for a sufficiently thin film. This thin film is a model for the complex corneal surface, which is wet by the aqueous fluid. The small flux of fluid inside the thin part of the film is believed to be similar to the flow that may occur in the hydrated mucus at the corneal surface.

We found that the 'dryspots' resulting from evaporation first appeared in the black line and then widened. A second dry region could open from the centre of the film; the spot in the middle of the film widens much more rapidly than the black line region. These spots behave similarly to those observed *in vivo*. Though dry patches resulting from tear film break-up *in vivo* are somewhat irregular, a rough estimate of the opening speed is of similar magnitude to the results from our computations when the combination of parameters governing evaporation and van der Waals forces (i.e. $h_{\mathrm{eq}} = (\delta A)^{1/3}$) is chosen to be a reasonable thickness compared with the thickness of the mucin-rich area at the corneal surface. We take this result to be encouraging for studying the model further in the context of blink cycle modelling and in 2D domains. Tear film dynamics on 2D eye-shaped domains, without conjoining pressure or evaporation, have already been studied (Maki *et al.* 2010a,b). A study for the model developed in this paper on a 2D eye-shaped domain is currently underway.

Acknowledgement

RJB thanks Dr P.E. King-Smith for helpful discussions and for sharing data.

Funding

US National Science Foundation, Computational Science Training for Undergraduates in the Mathematical Sciences (DMS-0639300 to K.N.W. and D.M.A.), (DMS-0709095 to D.M.A.) and (DMS-0616483 to R.J.B.).

REFERENCES

AJAEV, V. S. (2005a) Evolution of dry patches in evaporating liquid films. *Phys. Rev. E*, **72**, 031605.

AJAEV, V. S. (2005b) Spreading of thin volatile liquid droplets on uniformly heated surfaces. *J. Fluid Mech.*, **528**, 279–296.

AJAEV, V. S. & HOMSY, G. M. (2001) Steady vapor bubbles in rectangular microchannels. *J. Colloid Interface Sci.*, **240**, 259–271.

BRAUN, R. J. & FITT, A. D. (2003) Modeling the drainage of the precorneal tear film after a blink. *Math. Med. Biol.*, **20**, 1–28.

BRAUN, R. J. & KING-SMITH, P. E. (2007) Model problems for the tear film in a blink cycle: single equation models. *J. Fluid Mech.*, **586**, 465–490.

BRON, A. J., TIFFANY, J. M. & GAFFNEY, E. A. (2008) Compartmental factors influencing tear film osmolarity. *Acta Ophthalmol.*, **86**, 4333. doi: 10.1111/j.1755-3768.2008.4333.x.

BRON, A. J., TIFFANY, J. M., GOUVEIA, S. M., YOKOI, N. & VOON, L. W. (2004) Functional aspects of the tear film lipid layer. *Exp. Eye Res.*, **78**, 347–360.

BURELBACH, J. P., BANKOFF, S. G. & DAVIS, S. H. (1988) Nonlinear stability of evaporating/condensing liquid films. *J. Fluid Mech.*, **195**, 463–494.

CHER, I. (2007) Another way to think of tears: blood, sweat, and . . . "dacruon". *Ocul. Surf.*, **5**, 251–254.

CREECH, J. L., DO, L. T., FATT, I. & RADKE, C. J. (1998) *In vivo* tear-film thickness determination and implications for tear-film stability. *Curr. Eye Res.*, **17**, 1058–1066.

GIPSON, I. K. (2004) Distribution of mucins at the ocular surface. *Exp. Eye Res.*, **78**, 379–388.

GORLA, M. S. R. & GORLA, R. S. R. (2004) Rheological effects of tear film rupture. *Int. J. Fluid Mech. Res.*, **31**, 552–562.

JONES, M. B., PLEASE, C. P., MCELWAIN, D. L. S., FULFORD, G. R., ROBERTS, A. P. & COLLINS, M. J. (2005) Dynamics of tear film deposition and draining. *Math. Med. Biol.*, **22**, 265–288.

KING-SMITH, P. E., FINK, B. A., FOGT, N. NICHOLS, K. K., HILL, R. M. & WILSON, G. S. (2000) The thickness of the human precorneal tear film: evidence from reflection spectra. *Invest. Ophthalmol. Vis. Sci.*, **41**, 3348–3359.

KING-SMITH, P. E., FINK, B. A., HILL, R. M., KOELLING, K. W. & TIFFANY, J. M. (2004) The thickness of the tear film. *Curr. Eye Res.*, **29**, 357–368.

KING-SMITH, P. E., FINK, B. A., NICHOLS, J. J., NICHOLS, K. K., BRAUN, R. J. & MCFADDEN, G. B. (2009) The contribution of lipid layer movement to tear film thinning and breakup. *Invest. Ophthalmol. Vis. Sci.*, **50**, 2747–2756.

KING-SMITH, P. E., NICHOLS, J. J., NICHOLS, K. K., FINK, B. A. & BRAUN, R. J. (2008) Contributions of evaporation and other mechanisms to tear film thinning and breakup. *Optom. Vis. Sci.*, **85**, 623–630.

KLYCE, S. D. & RUSSELL, S. R. (1979) Numerical solution of coupled transport equations applied to corneal hydration dynamics. *J. Physiol.*, **292**, 107–134.

LEMP, M. A., BAUDOUIN, C., BAUM, J., DOGRU, M., FOULKS, G. N., KINOSHITA, S., LAIBSON, P., MCCULLEY, J., MURUBE, J., PFLUGFELDER, S. C., ROLANDO, M. & TODA, I. (2007) The definition and classification of dry eye disease: report of the Definition and Classification Subcommittee of the International Dry Eye WorkShop 2007. *Ocul. Surf.*, **5**, 75–92. Available at http://www.theocularsurface.com/DEWSReport.htm.

LEVIN, M. H. & VERKMAN, A. S. (2004) Aquaporin-dependent water permeation at the mouse ocular surface: in vivo microfluorimetric measurements in cornea and conjunctiva. *Invest. Ophthalmol. Vis. Sci.*, **45**, 4423–4432.

MAKI, K. L., BRAUN, R. J., HENSHAW, W. D. & KING-SMITH, P. E. (2010a) Tear film dynamics on an eye-shaped domain I: pressure boundary conditions. *Math. Med. Biol.*, **27**, 227–254.

MAKI, K. L., BRAUN, R. J., UCCIFERRO, P., HENSHAW, W.D. & KING-SMITH, P. E. (2010b) Tear film dynamics on an eye-shaped domain II: flux boundary conditions. *J Fluid Mech*, **647**, 361–390.

MATHERS, W. (2004) Evaporation from the ocular surface. *Exp. Eye Res.*, **78**, 389–394.

MCCULLEY, J. P. & SHINE, W. E. (1997) A compositional model for the tear film lipid layer. *Trans. Am. Ophthalmol. Soc.*, **95**, 79–93.

MISHIMA, S. (1965) Some physiological aspects of the precorneal tear film. *Arch. Ophthalmol.*, **73**, 233–241.

MISHIMA, S. & MAURICE, D. M. (1961) The oily layer of the tear film and evaporation from the corneal surface. *Exp. Eye Res.*, **1**, 39–45.

NAIRE, S., BRAUN, R. J. & SNOW, S. A. (2000) Limiting cases of gravitational drainage of a vertical free film for evaluating surfactants. *SIAM J. Appl. Math.*, **61**, 889–913.

PURSLOW, C. & WOLFFSOHN, J. S. (2005) Ocular surface temperature: a review. *Eye Contact Lens*, **31**, 117–123.

ROLANDO, M. & REFOJO, M. F. (1983) Tear evaporimeter for measuring water evaporation rate from the tear film under controlled conditions in humans. *Exp. Eye Res.*, **36**, 25–33.

SHARMA, A. (1998) Acid-base interactions in the cornea-tear film system: surface chemistry of corneal wetting, cleaning, lubrication, hydration and defense. *J. Dispers. Sci. Technol.*, **19**, 1031–1068.

SHARMA, A., TIWARI, S., KHANNA, R. & TIFFANY, J. M. (1998) Hydrodynamics of meniscus-induced thinning of the tear film. *Lacrimal Gland, Tear Film, and Dry Eye Syndrome 2* (D. A. Sullivan, D. A. Dartt & M. A. Meneray, eds). New York: Plenum, pp. 425–431.

SHARMA, A. (2003) Many paths to dewetting of thin films: anatomy and physiology of surface instability. *Eur. Phys. J. E*, **12**, 397–408.

SHARMA, A., KHANNA, R. & REITER, G. (1999) A thin film analog of the corneal mucus layer of the tear film: an enigmatic long range non-classical DLVO interaction in the breakup of thin polymer films. *Colloids Surf. B*, **14**, 223–235.

SHARMA, A. & RUCKENSTEIN, E. (1985) Mechanism of tear film rupture and formation of dry spots on cornea. *J. Colloid Interface Sci.*, **106**, 12–27.

SMITH, J. A., ALBEITZ, J., BEGLEY, C., CAFFERY, B., NICHOLS, K., SCHAUMBERG, D. & SCHEIN, O. (2007) The epidemiology of dry eye disease: report of the Epidemiology Subcommittee of the International Dry Eye WorkShop 2007. *Ocul. Surf.*, **5**, 93–107. Available at http://www.theocularsurface.com/DEWSReport.htm.

THIELE, U., BRUSCH, L., BESTEHORN, M. & BAR, M. (2003) Modelling thin-film dewetting on structured substrates and templates: bifurcation analysis and numerical simulations. *Eur. Phys. J. E*, **11**, 255–271.

TIFFANY, J. M. (1987) The lipid secretion of the meibomian glands. *Adv. Lipid Res.*, **22**, 1–62.

TIFFANY, J. M. (1991) The viscosity of human tears. *Int. Ophthalmol.*, **15**, 371–376.

WANG, J., FONN, D., SIMPSON, T. L. & JONES, L. (2003) Precorneal and pre- and postlens thickness measured indirectly with optical coherence tomography. *Invest. Ophthalmol. Vis. Sci.*, **44**, 2006–2011.

WONG, H., FATT, I. & RADKE, C. J. (1996) Deposition and thinning of the human tear film. *J. Colloid Interface Sci.*, **184**, 44–51.

WU, Q. & WONG, H. (2004) A slope-dependent disjoining pressure for non-zero contact angles. *J. Fluid Mech.*, **506**, 157–185.

ZHANG, Y. L., MATAR, O. K. & CRASTER, R. V. (2003a) Analysis of tear film rupture: effect of non-Newtonian rheology. *J. Colloid Interface Sci.*, **262**, 130–148.

ZHANG, Y. L., MATAR, O. K. & CRASTER, R. V. (2003b) Surfactant driven flows overlying a hydrophobic epithelium: film rupture in the presence of slip. *J. Colloid Interface Sci.*, **264**, 160–175.

ZHANG, Y. L., MATAR, O. K. & CRASTER, R. V. (2004) Rupture analysis of the corneal mucus layer of the tear film. *Mol. Simul.*, **30**, 167–172.